Atomic ionization by intense laser pulses of short duration: Photoelectron energy and angular distributions

M. Dondera

University of Bucharest, Faculty of Physics, Bucharest-Magurele 077125, Romania

(Received 24 July 2009; revised manuscript received 31 October 2010; published 30 November 2010)

We introduce an adequate integral representation of the wave function in the asymptotic region, valid for the stage postinteraction between a one-electron atom and a laser pulse of short duration, as a superposition of divergent radial spherical waves. Starting with this representation, we derive analytic expressions for the energy and angular distributions of the photoelectrons and we show their connection with expressions used before in the literature. Using our results, we propose a method to extract the photoelectron distributions from the time dependence of the wave function at large distances. Numerical results illustrating the method are presented for the photoionization of hydrogenlike atoms from the ground state and several excited states by extreme ultraviolet pulses with a central wavelength of 13.3 nm and several intensities around the value $I_0 \approx 3.51 \times 10^{16}\ \mathrm{W/cm^2}$.

DOI: 10.1103/PhysRevA.82.053419 PACS number(s): 32.80.Rm, 32.80.Fb

I. INTRODUCTION

Many theoretical studies [1] aiming to the accurate description of the photoionization or photodetachment of atomic systems in interaction with laser pulses rely on the numerical integration of time-dependent Schrödinger equation (TDSE) by grid (or combined grid spectral) methods. In principle all the quantities which characterize the emitted electrons can be determined from the wave function, once its dependence on coordinates and time is known. In practice the problem of extraction of the photoelectron distributions from the wave function is not a trivial one, especially in the case of a many-electrons system, and its solution is strongly influenced by the representation used for the wave function.

To solve the mentioned problem several methods were developed along the years. A first group of methods [2,3] uses the information contained in the wave packet at a fixed time, conveniently chosen after the conclusion of the laser pulse. To fix the ideas we refer to the most detailed photoelectron distribution, fully differential in energies *and* emission directions or, equivalently, in photoelectron kinetic momenta. This distribution can be determined by projecting the wave function on continuum states with adequate asymptotic behavior, namely satisfying the incoming-wave boundary condition [4]. However, the numerical calculation of these states for complex atomic systems is itself a complicated problem [5], sometimes comparable as difficulty with the integration of TDSE. In Ref. [3] a practical method was presented to extract the photoelectron kinetic momentum distribution from the wave function by appropriate projections in restricted regions of the space. The procedure allows one to replace the exact continuum states for the original problem by either Coulomb or free particle continuum states.

We mention that for the photoelectron energy spectrum, a less detailed distribution, there are known efficient calculation methods, like, for example, the window operator method (see Ref. [2]), which do not require the explicit building of the continuum states.

A second group of methods exploits the information contained in the time dependence of the wave function. The possibility to calculate the photoelectron angular distribution by the time integration of the probability current, involving the knowledge of the wave function at large distances, was frequently used. An interesting approach, relating the Fourier spectrum of the wave function autocorrelation and the energy spectrum, was developed in [6]. The same paper also presents a recipe to separate the contribution of the various partial waves to the spectrum. "Virtual detector" methods, quantal [7] or based on semiclassical assumptions [8], were also proposed and applied to determine the electron momentum distribution. A method of a different type, designed to extract the amplitudes for single and double ionization from the wave packet, was presented in [9]. These amplitudes are computed using the solution of a driven time-independent equation, where the driving term is represented by the wave function at the end of the radiation pulse (emulating in fact the TDSE integration over an infinite duration).

In this paper we propose yet a procedure to determine the photoelectron distributions, which uses the time dependence of the wave function in the asymptotic region, fully avoiding the explicit use of (exact or approximate) continuum states. At formal level, our procedure is closest to that of Ref. [7], with differences coming from the study of different processes. In Sec. II we first introduce by Eq. (2) an appropriate representation for the wave function in terms of divergent radial spherical waves, valid at large distances from the atomic core and after the end of the laser pulse. We show the connection of the amplitude of these spherical waves with the coefficients in the expansion of the wave function in terms of stationary solutions of the Schrödinger equation, then we obtain the photoelectron distributions we are looking for. The most differential distribution is given by Eq. (12).

In Sec. III we develop a numerical method to determine the photoelectron distributions, based on Eq. (12). The method relies on the numerical integration of TDSE, followed by the extraction of the photoelectron distributions from the time dependence of the wave function on the confines of the spatial region used for TDSE integration. We compare the present method with the procedure of projecting the wave packet on incoming continuum states, then in Sec. IV we apply our method to the case of a hydrogenlike atom exposed to an intense extreme ultraviolet (xuv) laser pulse and we present as graphs our numerical results for the photoelectron

distributions. The laser pulse parameters (wavelength and intensity) are in the same ranges as those corresponding to the pulses used in recent experiments described in Refs. [10,11], done at the new free-electron laser in Hamburg (FLASH). In these experiments surprising results were obtained for the photoionization of a Xenon gaseous target at intensities approaching I_0 and for wavelengths in the extreme ultraviolet range. The strong nonlinearity of the photoionization versus laser intensity (tens of photons absorbed per pulse by a Xenon atom) seems to indicate new facets of light-matter interaction. A first theoretical interpretation of the experimental results in Ref. [10], within perturbation theory using multiphoton ionization cross sections obtained through a scaling technique, was presented in Ref. [12].

Besides the illustration of the method, the aim of our numerical simulations is to generate results which may contribute to the understanding of the photoionization mechanism for xuv pulses of high intensity. In particular, we explore the role of excess photonionization and resonances, for xuv pulses similar to those considered in [10,11]. In our opinion precise results for "simple" systems are still of considerable interest for the current stage of theoretical description: they can help validate of the various working hypotheses adopted for the description of complex atomic systems and they can support the deciphering of finer details of the future photoionization experiments.

Atomic units (a.u.) are used throughout this paper unless specified otherwise.

II. PHOTOELECTRON ENERGY AND ANGULAR DISTRIBUTIONS

We consider an electron moving in an atomic potential $V(\boldsymbol{r})$ which supports at least one bound state. Our system, assumed as being initially in a bound state or in a superposition of bound states, interacts with an intense laser pulse on a finite time interval $t_i < t < t_f$. The quantitative description of the photoionization is expressed by various probability distributions like the photoelectron energy spectrum, the angular distribution or, in more detail, the angle-resolved energy distribution.

As mentioned in Sec. I, we are interested to compute the photoelectron distributions without resorting to the projection of the wave function on continuum states. In the following we relate the computation of the distributions to the behavior of the wave function $\psi(\boldsymbol{r},t)$ for $r \to \infty$ and after the interaction with the laser pulse, in correspondence with the direct experimental evaluation of these quantities, which involves measurements made usually at *large* distances from the target.

The outline of this section is as follows: (i) Starting with the behavior of the wave function at large distances expressed as in Eq. (2) and using the general expansion of the wave function in terms of energy eigenfunctions, we obtain Eq. (6), an expression for the photoelectron energy spectrum; (ii) we derive then, using the expression of the density of probability current, a formula for the angular distribution, Eq. (8); (iii) we interpret the results and we reach Eq. (9) for the fully differential distribution; and (iv) we derive Eq. (12), representing the receipt we use for computing the angle-resolved photoelectron energy spectrum from the temporal Fourier transform of the wave function in the asymptotic region.

The asymptotic behavior of the wave function for $t > t_f$ follows from the fact that at large distances from the origin the photoelectron is practically free and moves away from the nucleus. This implies that for every radial direction the wave function $\psi(\boldsymbol{r},t)$ can be written as a superposition of *divergent* radial spherical waves $e^{i(kr-Et)}/r$, where $k > 0$ and $E = k^2/2$. It is intuitively clear that the convergent waves $e^{i(-kr-Et)}/r$ should not contribute, as these would describe electrons coming from infinity toward the origin. That this is the case can be justified by analyzing the evolution in time of the corresponding wave packets. We work with a *reduced* wave function,

$$F(\boldsymbol{r},t) \equiv r\,\psi(\boldsymbol{r},t), \tag{1}$$

and we write its asymptotic behavior, guided by the aforementioned considerations, as follows:

$$F(\boldsymbol{r},t) \;\to\; \frac{1}{\sqrt{2\pi}} \int_0^\infty f(E,\boldsymbol{n})\, e^{i(kr-Et)}\, dE\,, \;\; r \to \infty, \tag{2}$$

with $\boldsymbol{n} \equiv \boldsymbol{r}/r$. The right-hand side of this equation is a wave packet moving in outward radial direction. The amplitude $f(E,\boldsymbol{n})$ of a wave from the packet depends on photoelectron energy E and this dependence changes with the radial direction $\boldsymbol{n}$. It will become evident in the following that this quantity contains the whole information about photoionization. We note that Eq. (2) is written for a potential which decreases at large distances faster than $1/r$. We discuss at the end of this section the modifications for the case of a potential having a Coulomb tail.

In order to express the probability density of the photoelectron energy by the amplitude $f(E,\boldsymbol{n})$ from Eq. (2) we expand the wave function, after the end of the laser pulse, in terms of stationary solutions of TDSE, then we consider its asymptotic behavior. We use the two familiar complete systems of energy eigenfunctions, one composed from the set $\{u_j(\boldsymbol{r})\}$, the eigenfunctions corresponding to the energies in the discrete spectrum, together with $\{u^{(-)}(\boldsymbol{k},\boldsymbol{r})\}$ and the other one composed from the set $\{u_j(\boldsymbol{r})\}$ together with $\{u^{(+)}(\boldsymbol{k},\boldsymbol{r})\}$. The functions $u^{(-)}(\boldsymbol{k},\boldsymbol{r})$ and $u^{(+)}(\boldsymbol{k},\boldsymbol{r})$ are the continuum eigenfunctions, asymptotically behaving as a superposition of a plane wave and a *convergent*, respectively, *divergent* spherical wave, and normalized in the wave vector $\boldsymbol{k}$ scale. In the mentioned expansions,

$$\psi(\boldsymbol{r},t) = \sum_j c_j\, u_j(\boldsymbol{r})\, e^{-iE_j t} + \int c^{(\mp)}(\boldsymbol{k})\, u^{(\mp)}(\boldsymbol{k},\boldsymbol{r})\, e^{-iEt}\, d\boldsymbol{k}, \tag{3}$$

all the coefficients are constant in time and, of course, $c^{(+)}(\boldsymbol{k})$ and $c^{(-)}(\boldsymbol{k})$ are not independent.

The relations,

$$f(E,\boldsymbol{n}) = -i\, c^{(-)}(k\boldsymbol{n}), \tag{4}$$

and

$$f(E,\boldsymbol{n}) = -i\left[c^{(+)}(k\boldsymbol{n}) + \frac{ik}{2\pi}\int_{4\pi} f^{(+)}(\boldsymbol{k},\boldsymbol{n})\, c^{(+)}(\boldsymbol{k})\, d\Omega_{\hat{\boldsymbol{k}}}\right], \tag{5}$$

connecting the amplitude $f(E,\boldsymbol{n})$ and the expansion coefficients $c^{(\mp)}(\boldsymbol{k})$, follow from the comparison of Eq. (2) with Eq. (3) taken at large distances and long times. In the last expression $f^{(+)}(\boldsymbol{k},\boldsymbol{n})$ is the elastic scattering amplitude on the potential $V(\boldsymbol{r})$.

As being an expansion over energy eigenfunctions, Eq. (3) gives directly the energy distribution $dp(E)$ of the electron; for $E>0$ it follows either as $dp(E)=k[\int_{4\pi}|c^{(-)}(k\boldsymbol{n})|^2 d\Omega]dE$, or as $dp(E)=k[\int_{4\pi}|c^{(+)}(k\boldsymbol{n})|^2 d\Omega]dE$, with the solid angle element $d\Omega$ around the direction $\boldsymbol{n}$ [13]. Using now Eq. (4) it follows that

$$dp(E)=k\left[\int_{4\pi}|f(E,\boldsymbol{n})|^2 d\Omega\right]dE. \tag{6}$$

The relation (6) expresses the photoelectron energy spectrum by the amplitude $f(E,\boldsymbol{n})$.

To determine the photoelectron angular distribution we start from the total probability $dp(\boldsymbol{n})$ that the electron crosses a surface element $d\boldsymbol{S}=\boldsymbol{n}\,r^2\,d\Omega$ at the asymptotic position $\boldsymbol{r}=r\,\boldsymbol{n}$. We obtain this probability integrating in time the product $\boldsymbol{J}(\boldsymbol{r},t)\cdot d\boldsymbol{S}$, where $\boldsymbol{J}(\boldsymbol{r},t)$ is the density of probability current. The integral is extended over the time interval (t_1,t_2) in which the wave function $\psi(\boldsymbol{r},t)$ and, together with it, $\boldsymbol{J}(\boldsymbol{r},t)$ take non-negligible values at the position $\boldsymbol{r}$. For a given laser pulse and a given initial state these moments depend solely on $\boldsymbol{r}$. In order to use the expression of $\boldsymbol{J}$ in the *absence* of the electromagnetic field we have to ensure the condition $t_1\geqslant t_f$, which can always be realized for large enough r. More precisely, this condition is satisfied if we take $r\geqslant a$, with a defined such that the probability to find the electron outside the sphere of radius a, at the moment t_f, is negligible. Using the well-known expression of $\boldsymbol{J}$ [14], we obtain

$$dp(\boldsymbol{n})=\mathrm{Im}\left[\int_{t_1}^{t_2}F^*(\boldsymbol{r},t)\,\frac{\partial F(\boldsymbol{r},t)}{\partial r}\,dt\right]d\Omega. \tag{7}$$

This relation connects the photoelectron angular distribution and the reduced wave function. After using the function F and its complex conjugate according to the asymptotic formula (2), the resulting temporal integral takes the form $\int_{t_1}^{t_2}\exp[i(E-E')t]\,dt$. Letting the duration t_2-t_1 to increase to infinity [it is possible to do so since $F(\boldsymbol{r},t)$ is negligible outside the interval (t_1,t_2)], this integral becomes $2\pi\delta(E-E')$. Then one of the integrals in energy can also be done and we obtain the relation:

$$dp(\boldsymbol{n})=\left[\int_0^\infty k\,|f(E,\boldsymbol{n})|^2\,dE\right]d\Omega, \tag{8}$$

expressing the photoelectron angular distribution by the amplitude $f(E,\boldsymbol{n})$.

The photoelectron energy spectrum (6) and the angular distribution (8) are obtained by the integration of the same *positive* quantity over emission directions and energies, respectively. The aspect of these equations compels us to interpret the quantity,

$$d^2p=k\,|f(E,\boldsymbol{n})|^2\,dE\,d\Omega, \tag{9}$$

as the emission probability of a photoelectron with an energy in $(E,E+dE)$, in a direction $\boldsymbol{n}$ of a solid angle element $d\Omega$. Equivalently, expressing the volume element in momentum space as $d\boldsymbol{k}=k\,dE\,d\Omega$, we interpret the quantity $|f(E,\boldsymbol{n})|^2\,d\boldsymbol{k}$ as the probability to find a value for the photoelectron kinetic momentum in $d\boldsymbol{k}$.

The relation (9) describes the *fully* differential distribution, in energies and emission directions of the photoelectron. This distribution is calculated from the ionization amplitude $f(E,\boldsymbol{n})$ introduced through Eq. (2). It is then necessary to find practical ways to extract this amplitude from the wave function.

Before describing our procedure, we remark that Eq. (4) allows us to rewrite Eq. (9) as follows:

$$d^2p=|c^{(-)}(\boldsymbol{k})|^2\,d\mathbf{k}=\left|\int u^{(-)*}(\boldsymbol{k},\boldsymbol{r})\,\psi(\boldsymbol{r},t)\,d\boldsymbol{r}\right|^2 d\boldsymbol{k}. \tag{10}$$

This relation, valid for any time $t\geqslant t_f$, was applied many times [15] and expresses the property that $|c^{(-)}(\boldsymbol{k})|^2$ is the probability density of the photoelectron kinetic momentum. We note that $|c^{(+)}(\boldsymbol{k})|^2=|\int u^{(+)*}(\boldsymbol{k},\boldsymbol{r})\,\psi(\boldsymbol{r},t)\,d\boldsymbol{r}|^2$ does not have the same significance as $|c^{(-)}(\boldsymbol{k})|^2$. This shows the special role of the *incoming* waves $u^{(-)}(\boldsymbol{k},\boldsymbol{r})$ for the description of the photoionization process. To determine only the energy spectrum we can project equally well on the *outgoing* waves $u^{(+)}(\boldsymbol{k},\boldsymbol{r})$ [see the paragraph including Eq. (6)].

As the procedure based on the projection of the wave packet on $u^{(-)}(\boldsymbol{k},\boldsymbol{r})$ implies the preliminary determination of these eigenfunctions and raises delicate numerical problems, we focus on the possibility to completely avoid the use of continuum states. In this purpose, we return to Eq. (2) and we note that, for a given position vector $\boldsymbol{r}$, with $r\to\infty$, the correspondence between F (as function of time) and f (as function of energy) may be inverted, the result being

$$f(E,\boldsymbol{n})=\frac{e^{-ikr}}{\sqrt{2\pi}}\int_{t_1}^{t_2}F(\boldsymbol{r},t)\,e^{iEt}\,dt, \tag{11}$$

where the function $F(\boldsymbol{r},t)$ is supposed as previously mentioned [see the context of Eq. (7)] to be negligible outside the interval (t_1,t_2), with $t_1\geqslant t_f$. Replacing the ionization amplitude $f(E,\boldsymbol{n})$ in Eq. (9) we obtain the compact result,

$$d^2p=\frac{k}{2\pi}\left|\int_{t_1}^{t_2}F(\boldsymbol{r},t)\,e^{iEt}\,dt\right|^2 dE\,d\Omega\,, \tag{12}$$

connecting the probability distribution with the temporal Fourier transform of the reduced wave function $F(\boldsymbol{r},t)$ at *large* distances.

We mention that Eq. (12) remains valid also for a potential of Coulomb type at large distances, $V(\boldsymbol{r})\to-Z/r$, for $r\to\infty$, a property which can be understood if we examine what become Eqs. (2) and (11) in this case (the intermediate equations are not affected by the Coulomb tail of the potential). They are replaced, respectively, by

$$F(\boldsymbol{r},t)\to\frac{1}{\sqrt{2\pi}}\int_0^\infty f(E,\boldsymbol{n})\,e^{i(kr+\eta\ln 2kr-Et)}\,dE,\quad r\to\infty, \tag{13}$$

with $\eta\equiv Z/k$, and

$$f(E,\boldsymbol{n})=\frac{e^{-i(kr+\eta\ln 2kr)}}{\sqrt{2\pi}}\int_{t_1}^{t_2}F(\boldsymbol{r},t)\,e^{iEt}\,dt,\quad r\to\infty. \tag{14}$$

The phase factor in front of the integral disappears when taking the squared modulus and, consequently, Eq. (12) keeps its form unchanged.

By the integration of Eq. (9) we can find the other related distributions, Eqs. (6) and (8), and the total ionization probability,

$$P_{\rm ion} = \int_0^\infty \int_{4\pi} k\,|f(E,\boldsymbol{n})|^2\,dE\,d\Omega. \tag{15}$$

From $P_{\rm ion}$ one can calculate the survival probability of the atom as $P_{\rm surv} = 1 - P_{\rm ion}$, relation which may also serve for numerical verification if $P_{\rm surv}$ can be evaluated in an independent way.

We finally remark that Eq. (12) is not restricted to photoionization only: it applies to any other ionization process of a one-electron atom from an initial bound state, due to an interaction with finite duration.

III. NUMERICAL METHOD

After describing our method to determine the photoelectron distributions, based on the use of Eq. (12), we mention several calculations we made in order to test its accuracy. A comparison of our method and that based on Eq. (10) follows. In the next section we present our results concerning the photoionization of hydrogenlike atoms.

We integrate numerically the time-dependent Schrödinger equation on a space domain composed from an inner region $\mathcal{D}$, chosen such that it contains at the conclusion of the laser pulse the whole wave function, and an outer region $\mathcal{D}'$, whose role is to absorb the wave function using a mask function or an absorbing potential. The integration of TDSE begins from the chosen initial state and is continued after the end of the pulse until the continuum part of the wave function escapes from $\mathcal{D}$. From the time dependence of the reduced wave function $F(\boldsymbol{r},t)$ on the confines of $\mathcal{D}$, recorded during the TDSE integration, we calculate its temporal Fourier transform and the angle-resolved photoelectron energy distribution (12). The other distributions are then obtained by integration over photoelectron energies [Eq. (8)] or emission directions [Eq. (6)]. In practice the simplest choice of the inner region $\mathcal{D}$ is that of a sphere, of radius a. An estimation for the radius a may be derived from the condition that the fastest photoelectrons, treated as particles in free classical motion, generated near the nucleus at the beginning of the pulse, are still in $\mathcal{D}$ at the end of the pulse; the result is $a_{\rm cl} = 2\pi N_c \sqrt{2N_{\rm ph}/\omega}$, where N_c is the number of cycles of the laser pulse and $N_{\rm ph}$ is the maximum number of photons absorbed in excess by the photoelectron. The time duration $\tau_a \equiv t_2 - t_1$ used to analyze the wave packet is dictated by the lowest energy E_0 of the photoelectrons for which we want to predict results. An useful approximation of this duration is $\tau_{a;\rm cl} = a/\sqrt{2E_0}$.

For checking the accuracy of the present method we have made comparisons between distributions generated by our code and distributions known from literature [16], with satisfactory results.

Now we compare our method, that we conventionally name method I, and the method of projecting the wave packet on incoming energy eigenfunctions $u^{(-)}(\boldsymbol{k},\boldsymbol{r})$, involving Eq. (10) at the end of the laser pulse, that we name method II. In favor of method I we mention the simplicity, its application involving only the calculation of the temporal Fourier transform of the wave function, which can be made efficiently using FFT algorithms. It can be applied to noncentral potentials, with no major difficulties once the wave function is calculated. Method II requires a precise computation of the functions $u^{(-)}(\boldsymbol{k},\boldsymbol{r})$, a difficult task, and then the projection of the wave packet on them. An advantage of method II is that it can be applied right at the end of the interaction with the laser pulse, while method I requires an additional computing time τ_a for the free propagation of the wave packet after the termination of the laser pulse. However, in many situations this time can be kept to a reasonable fraction of total computing time (a typical value of this fraction in our calculations, reported below, is 0.4) and we expect the case of complex targets to be even more favorable. A potential advantage of method I versus method II, not exploited in this paper, is connected to the radius a of the radial box. Apparently both methods require an increasing value a with the pulse duration and if longer pulses are considered their use becomes impractical. However, a generalization of method I[1] is possible such that a could be kept fixed (independent on pulse duration), its value being determined only by the condition that the relevant atomic states are well represented inside $\mathcal{D}$.

Now we give some details, most of them being of interest also for the next section, about the systems for which the comparison was done. We consider an electron in a *central* potential, in interaction with a *linearly* polarized laser pulse. We have adopted two choices of the atomic potential: (a) the potential $V_1(r) = -[1 + (1+\kappa r)\exp(-2\kappa r)]/r$, with $\kappa = 17/16$ a.u., useful to describe the helium atom behavior [17] in the single active electron approximation (SAE), and (b) the point Coulomb potential $V_2(r) = -Z/r$ of a hydrogenlike atom with the atomic number Z.

The z axis of the reference frame, with the unit vector denoted by $\boldsymbol{e}_z$, is chosen along the laser polarization direction. The pulse is described by the vector potential:

$$\boldsymbol{A}(t) = \frac{F_0}{\omega}\,\boldsymbol{e}_z\,s(t)\cos\omega t, \tag{16}$$

where F_0 is the electric field amplitude, ω is the laser frequency, and $s(t)$ is the pulse envelope. The laser peak intensity is $I = F_0^2$. We worked with a flat top pulse whose envelope $s(t)$ increases from 0 to 1 as $\cos^2(\pi t/2\tau_{\rm on})$ for $-\tau_{\rm on} < t < 0$, remains equal to 1 for a duration $\tau_{\rm flat}$, then decreases to 0 as $\cos^2[\pi(t-\tau_{\rm flat})/2\tau_{\rm on}]$ for $\tau_{\rm flat} < t < \tau_{\rm on} + \tau_{\rm flat}$. The pulse is turned off in a time interval $\tau_{\rm off} = \tau_{\rm on}$. The parameters $\tau_{\rm on}$ and $\tau_{\rm flat}$ are chosen as integer multiples of the laser period $T = 2\pi/\omega$.

We exploit the cylindrical symmetry of the system around the z axis by choosing to work in spherical coordinates r, θ, and φ (with the z axis as polar axis). For the present case, the Schrödinger equation admits factorized solutions of the form $F(\boldsymbol{r},t) = X(r,\theta,t)\,\frac{e^{im\varphi}}{\sqrt{2\pi}}$, where the new reduced wave function $X(r,\theta,t)$ only depends on *two* spatial variables. These

[1]The generalization, which will be presented elsewhere, is based on the property that in the Kramers-Henneberger reference frame the photoelectron is *free* at large distances during the laser pulse.

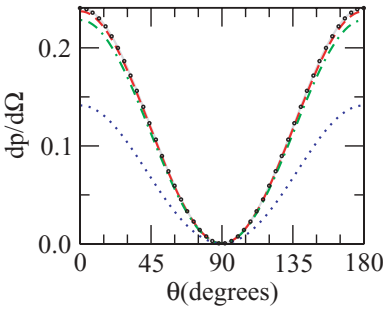

FIG. 1. (Color online) Photoelectron angular distribution for a ground-state helium atom (in SAE approximation) exposed to a flat top xuv pulse [Eq. (16)] with a peak intensity $I_3 = 10\,I_0$, the central frequency $\omega = 3.42$ a.u., and a total duration of 50 cycles. Four curves are obtained with method I [based on Eq. (12)] and correspond to the values 140 T (dotted line), 150 T (dot-dashed line), 155 T (dashed line), and 200 T (solid line) for the duration τ_a used to analyze the wave packet. The data represented by small circles are determined by method II [based on Eq. (10)].

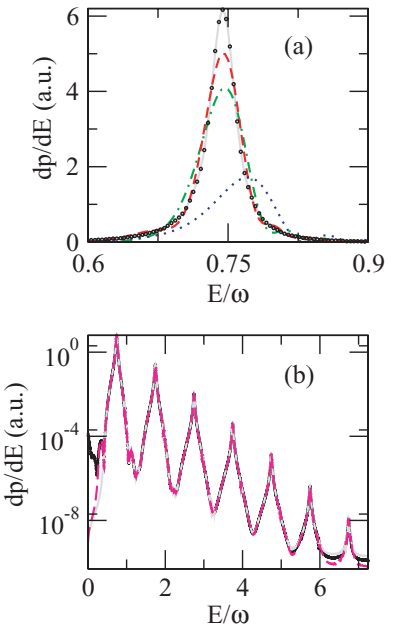

FIG. 2. (Color online) Photoelectron energy spectrum, as a function of the ratio between the photoelectron energy and the laser frequency, for the same system and laser pulse as in Fig. 1. Small circles represent the results obtained with method II. The other curves are obtained with method I, using in (a) the same durations τ_a as in Fig. 1, and the values 200 T (solid line) and 250 T (long dashed line) in (b).

solutions are suitable to satisfy the type of initial condition used in this paper: the atomic state before the pulse turns on is a stationary state with well-defined angular momentum. Inside the numerical code used to integrate TDSE (in velocity gauge) the wave function is alternatively represented either by its values $X(r,\theta,t)$ on a double grid in variables r and θ or by the values of its radial components $X_l(r,t)$ on the radial grid. The first representation is used to perform the radial propagation corresponding to the interaction between the atom and the laser field, the rest of the propagation being done in the second representation.

The numerical results we present were obtained for one value of the frequency, $\omega = 3.42$ a.u. (which corresponds to a wavelength of 13.3 nm), belonging to the xuv range, and for three values of the laser intensity, $I_1 = I_0/4.5$, $I_2 = I_0$, and $I_3 = 10\,I_0$, where $I_0 \approx 3.51 \times 10^{16}$ W/cm^2. We used a total pulse duration of 50 cycles (from which $\tau_{\rm on} = \tau_{\rm off} = 5\,T$ and $\tau_{\rm flat} = 40\,T$), in order to keep the running time to a reasonable value.

The comparison of methods I and II is illustrated in Figs. 1 and 2 and in Fig. 3, the latter presented in Sec. IV. The results from Figs. 1 and 2 refer to the ionization from the ground state in the case of potential $V_1(r)$ and for the laser intensity I_3. We have used the value $a = 750$ a.u. for the radius of the inner region $\mathcal{D}$ (a value slightly higher than the estimation $a_{cl} \approx 680$ a.u., calculated for the actual laser pulse and eight photons absorbed in excess by the electron) and a maximum duration of $250\,T$ for the free propagation of the electronic wave packet.

In Fig. 1 we present the photoelectron angular distributions obtained with the two methods. The results of method I are shown for four values of τ_a: 140 T (dotted line), 150 T (dot-dashed line), 155 T (dashed line), and 200 T cycles (continuous line). The results obtained with method II are marked by circles. We note the very good agreement between the results of the two methods for $\tau_a = 200\,T$ and also that the curve corresponding to $\tau_a = 155\,T$ represents a good approximation of these results.

In Fig. 2 we extend the comparison to the photoelectron energy spectra. The curves from the upper panel correspond to the same conditions as in Fig. 1. The results represented in the lower panel are determined with method I for $\tau_a = 200\,T$ (solid line) and $\tau_a = 250\,T$ (long dashed line), and with method II (circles). In panel (a) only the first photoelectron peak is represented. In panel (b) we adopted a semilogarithmic scale to represent the results in order to be able to show the whole spectrum. Very small discrepancies are observed at both ends of the energy spectrum. For the low-energy region these discrepancies are compatible with the estimations based on $\tau_{a;\rm cl}$, which indicate that correct predictions are expected for $E > 0.43\,\omega$ if $\tau_a > 238\,T$, and for $E > 0.33\,\omega$ if $\tau_a > 272\,T$. We note, however, that the contribution of the range $E \lesssim 0.45\,\omega$ to the total ionization probability is very small (less than 10^{-3}). For the other end of the spectrum very small differences, without any practical relevance, are visible in the region $E > 6\,\omega$.

IV. NUMERICAL RESULTS FOR HYDROGENLIKE ATOMS

In this section we present our results concerning the photoionization of hydrogen atom and of hydrogenlike ions under the influence of xuv pulses. As initial atomic states we have considered stationary states nlm with $n \leqslant 3$ and $m = 0$. For all these initial states the angular distributions are symmetric around $\theta = 90^\circ$ and have peak values along the polarization axis. The number of minima of the angular distribution is

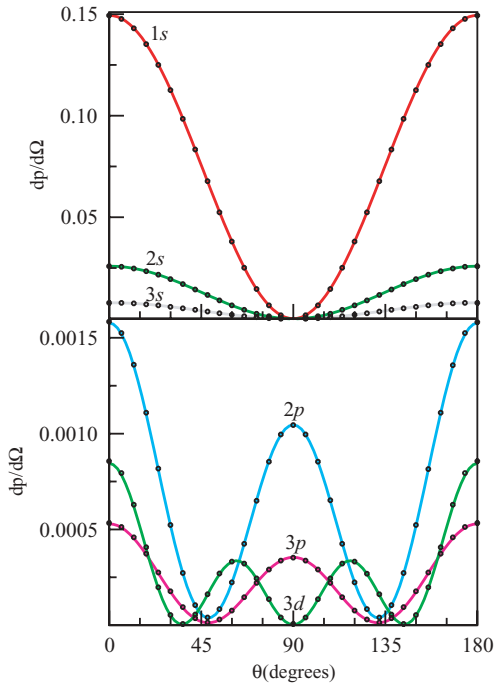

FIG. 3. (Color online) Photoelectron angular distributions for a hydrogen atom exposed to the same laser pulse as in Fig. 1. The results correspond to six different initial states, specified in the figure. For the case of the $3d$ initial state the ordinates are amplified by a factor of 100. For every initial condition two sets of data are represented, obtained using method I with $\tau_a = 250\,T$ (solid line) and method II (small circles).

generally $l + 1$ for all the situations investigated.[2] For initial states of type ns, in particular, the single minimum present is located at $\theta = 90°$. We first present results for the hydrogen atom ($Z = 1$) and for the laser intensity $I_3 = 10\,I_0$.

In Fig. 3 we show the photoelectron angular distributions corresponding to the initial states $1s$, $2s$, $2p$, $3s$, $3p$, and $3d$, the values for the case of the $3d$ initial state being multiplied by a factor of 100. The agreement between the results obtained with method I (solid line) for a duration of analysis of 250 T, and those obtained with method II (circles) is similar with that encountered in the case of Fig. 1.

The photoelectron distributions presented in Figs. 4–6 are determined using our method (method I). In Fig. 4 we show the energy spectrum for the same intensity and the same initial states as in Fig. 3. For a given initial state the peak height decreases monotonically and rapidly with the order of the peak [3]. The energies corresponding to the spectral maxima are

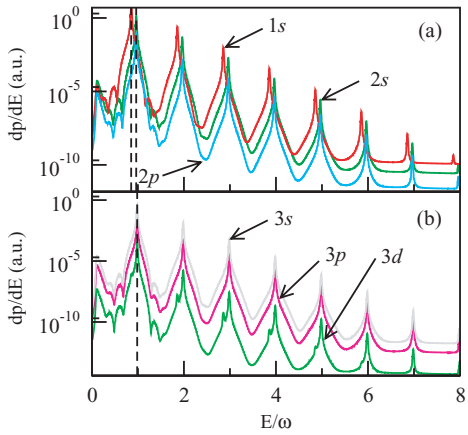

FIG. 4. (Color online) Photoelectron energy spectra, for the same conditions as in Fig. 3. The initial states are $1s$, $2s$, and $2p$ (a), and $3s$, $3p$, and $3d$ (b). The abscissas of the vertical dashed lines are calculated applying the energy conservation law to the ionization by one-photon absorption.

close to those given by the law of energy conservation for the case of a monochromatic field of low intensity (the latter are indicated by vertical dashed lines for the position of the first peak).

We now refer to the results we have obtained for the most detailed distribution, given by Eq. (12). In Fig. 5 we show, for $1s$, $2s$, and $2p$ initial states and laser intensity I_3, the angle-resolved photoelectron energy spectra for several directions, with $\theta = 5°, 45°, 60°$, and $90°$. We notice that these spectra are affected by the emission direction; both the relative magnitude and the number of the photoelectron energy peaks (in a given interval on the axis of ordinates) change significantly from the direction parallel with the polarization axis to a direction perpendicular on the same axis. The most pronounced changes of the spectrum manifest around $\theta = 90°$, where the only peaks which survive are: the second and the fourth for $1s$ and $2s$ initial states, and the first and the third for the $2p$ initial state (see also Footnote 2).

We mention that for laser intensities less than I_3 the photoelectron distributions are similar with those presented in Figs. 3–5. By lowering the laser intensity the weight of the excess photon ionization (EPI) decreases monotonically. To characterize quantitatively how important EPI is for the considered range of intensities we introduce the notation P_{n_0+s} for the probability of ionization with the absorption of $n_0 + s$ photons (n_0 being the minimum number of photons necessary for ionization, in our case one photon) and we examine the values of the ratio $\rho \equiv P_{\rm EPI}/P_{n_0}$, where $P_{\rm EPI} = \sum_{s>0} P_{n_0+s}$ is the probability of excess photon ionization. Even at high intensities, of the order of I_0, the ratio ρ is small compared to unity. In particular, in the case of $1s$ initial state, we obtained for ρ the values 3.45×10^{-2}, 3.45×10^{-3}, and 7.66×10^{-4}, corresponding to intensities I_3, I_2, and I_1, respectively. From

[2]The same number of minima is predicted by the lowest-order perturbation theory (LOPT) using the angular momentum selection rules. LOPT also explains correctly the absence of some peaks (those for which the number of photons absorbed and the angular momentum l of the initial state have different parities) in Figs. 5 and 6, for $\theta = 90°$.

[3]We did not try to achieve the numerical convergence of the spectra for energies corresponding to the last peaks (especially those for which the background begins to saturate), versus any parameter which may have impact on it. These last peaks are shown here [and in Figs. 2(b), 5, and 6] mainly to observe the data trend. We note that the oscillations induced by the spectral width of the pulse were smoothed replacing every ordinate (with the exception of those around the principal maxima) by its local arithmetic average, a procedure adopted also in the case of Figs. 2, 5, and 6.

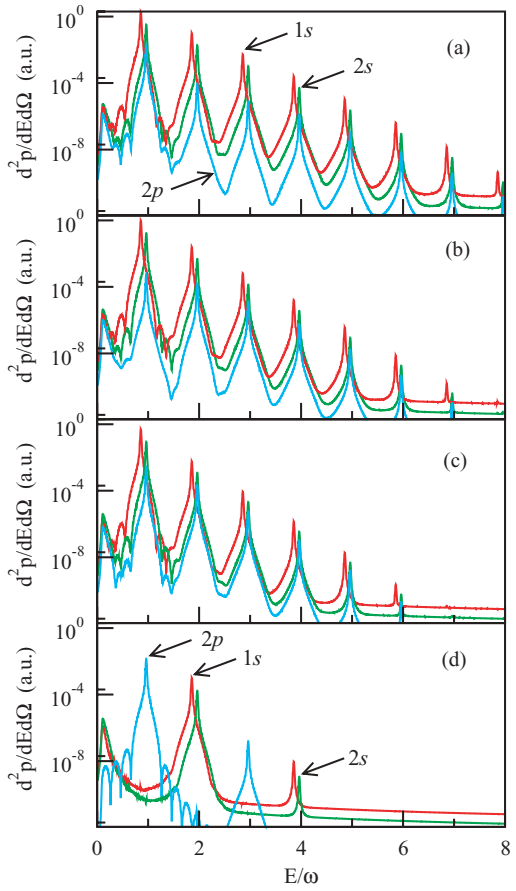

FIG. 5. (Color online) Angle-resolved photoelectron energy spectrum for the same conditions as in Fig. 3. The three curves from every panel correspond to $1s$, $2s$, and $2p$ initial states. From upper (a) to lower (d) panels, the values of angle θ are as follows: 5°, 45°, 60°, and 90°.

this numerical example, which seems to indicate a proportionality relation between ρ and I, we would be tempted to infer the validity of the power law, $P_{n_0+s} \sim I^{n_0+s}$, for the probability P_{n_0+s} as function of intensity. However, the ratio of the two values of P_{n_0} corresponding to intensities I_3 and I_2 is 5.91, very different from the ratio of intensities ($I_3/I_2 = 10$). This is a clear indication that it is necessary to include the depletion effect of the initial atomic state to correct the power law.

In the case of hydrogenlike ions we have at our disposal a parameter, the atomic number Z, which can be modified to achieve, for the same xuv pulse, the variation of the minimum number n_0 of photons required for ionization. This possibility can prove useful to a (at least) qualitative understanding of the sequential ionization of the atoms with many electrons. In the case of $Z = 1$ (Figs. 3–5), where the ionization potential of the ground state is 0.5 a.u., the laser frequency we have used (3.42 a.u.) in simulations is a high frequency. The same frequency should be considered a low one for a high Z ground-state hydrogenlike ion. The role of Z can be seen using the scaling rules of various quantities with the atomic number. These rules are obtained from the Schrödinger equation for a hydrogenlike atom with an atomic number Z by the variable changes $\tilde{\boldsymbol{r}} = Z\boldsymbol{r}$ and $\tilde{t} = Z^2 t$. This leads to the Schrödinger equation for the hydrogen atom in a laser pulse described again by Eq. (16) but with the frequency $\tilde{\omega} = \omega/Z^2$ and an electric field amplitude $\tilde{F}_0 = F_0/Z^3$. We mention that we preferred to use this transformation even for the numerical integration of TDSE: the numerical calculation was done for the hydrogen atom and the photoelectron distributions were correspondingly scaled. The energy spectrum, angle resolved or integrated, was divided by Z^2; this supplementary rule follows from Eq. (12) and from the normalization condition of the wave function.

In the following we present results obtained for the intensity I_3 and for three values of the atomic number, $Z = 2$, 3, and 5, the scaled frequency $\tilde{\omega}$ taking, respectively, the values 0.855, 0.38, and 0.1368 a.u.. The minimum number n_0 of photons required for ionization from the ground state is one for $Z = 2$, two for $Z = 3$, and increases to four for $Z = 5$. This fact has significant consequences for photoionization: For $Z = 2$ the atom is completely ionized at the conclusion of the laser pulse while the total ionization probability is 0.66 for $Z = 3$ and 0.01 for $Z = 5$. In Fig. 6 we show the angle-resolved photoelectron spectra for the initial state $1s$ and emission directions with $\theta = 15°, 30°, 45°, 60°, 75°$, and 90°. The three curves in every panel correspond to the mentioned values of the atomic number. Besides the differences concerning the position, the width and height of the peaks, we note their different structure. In the case $Z = 3$ every peak is split in several subpeaks of unequal magnitude. Three subpeaks are clearly visible and two of them are prominent. This distinctive feature is the consequence of the finite bandwidth of the pulse and of the (approximate) fulfillment of the resonance condition: the scaled frequency $\tilde{\omega} = 0.38$ a.u. is close to the energy difference of 0.375 a.u. between the levels $1s$ and $2p$ of the hydrogen atom. We note for the case $Z = 5$ a small (but visible) shift of the spectrum toward lower energies [see the relative position of the first peak versus the dashed line from panel (c)] and the nonmonotonic variation of the peaks height for some directions. At $\theta = 90°$ the peaks which survive are the second and the fourth for $Z = 2$ (like in the case $Z = 1$) and the first, the third, and the fifth for $Z = 3$ and $Z = 5$.

We mention that, in order to interpret the energy spectra from Fig. 6, we made independent calculations based on single-state Floquet theory (SSFT). The calculations were done with the numerical code STRFLO presented in [18]. In the framework of SSFT the behavior of an atom in a monochromatic laser field [4] is described by a quasistationary solution of TDSE, corresponding to a complex energy, termed quasienergy. A quasienergy which reduces in the absence of the field to an atomic level $E^{(0)}$ can be written as $E = E^{(0)} + \Delta - i\Gamma/2$, where Δ and Γ are the shift and width of the level, induced by the field. In SSFT the photoelectron energy spectrum is a "comb" formed by the lines corresponding to the energies $E^{(0)} + \Delta + (n_0 + s)\,\omega$, with s integer $\geqslant 0$. If several Floquet states are initially populated, then each of them contributes with its own comb to the photoelectron energy spectrum. In Fig. 7 we present an excerpt of the spectrum from panel (a) of Fig. 6, for photoelectron energies between $0.1\,\omega$ and $0.9\,\omega$. The relevant Floquet states in this context are proven to be those corresponding to the atomic states $1s$ for

[4] We note that the monochromaticity condition of the pulse described by Eq. (16) (in fact, of any pulse) is satisfied with approximation.

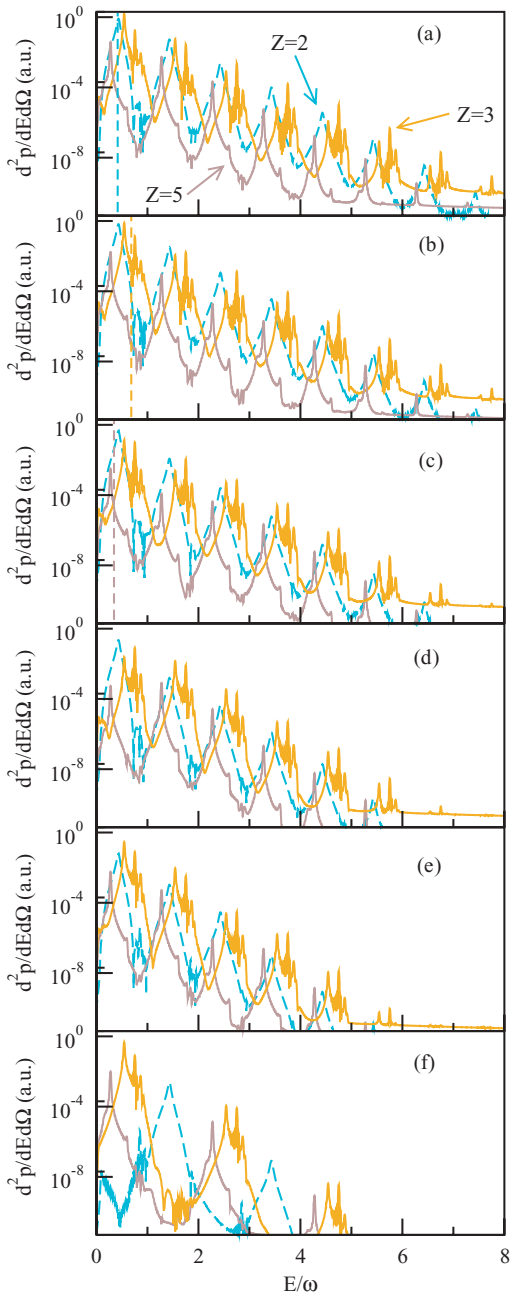

FIG. 6. (Color online) Angle-resolved photoelectron energy spectra for the same conditions as in Fig. 3 and for the $1s$ initial state. The three curves from every panel correspond to $Z = 2$, 3, and 5. From upper (a) to lower (f) panels, the values of angle θ are as follows: 15°, 30°, 45°, 60°, 75°, and 90°. The dashed lines, determined as in Fig. 4, are drawn once for every Z.

$Z = 2$ and $Z = 5$, and $1s$, $2p$, $3p$ in the case $Z = 3$. For every state involved, two vertical lines are drawn, their abscissas being $E_n/\omega + n_0$ (E_n is the corresponding Bohr level) for the dashed line and $(E_n + \Delta_{nl})/\omega + n_0$ for the solid line. From the left to the right, the first two pairs of vertical lines correspond, respectively, to the ground state for $Z = 5$ and $Z = 2$. The next three pairs of lines are for $Z = 3$ and correspond, respectively, to the states $2p$, $1s$, and $3p$. The figure clearly shows that the Floquet calculation reproduces with accuracy the position of peaks from the energy spectra. We note the negative value of

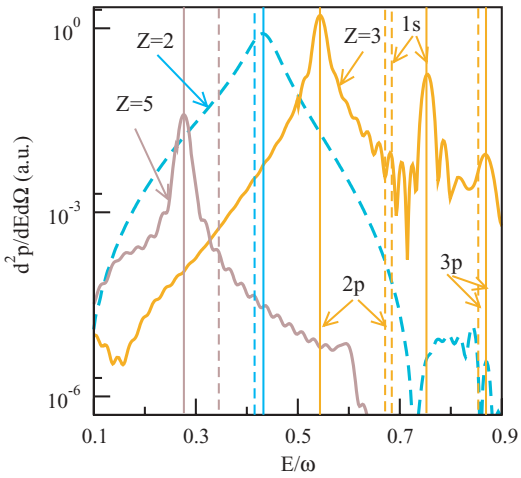

FIG. 7. (Color online) Magnification of the region between $E/\omega = 0.1$ and $E/\omega = 0.9$ from panel (a) of Fig. 6. The abscissas of vertical lines (two lines for every state) are calculated with the energy conservation law as explained in the text. The pairs of lines correspond (from left to right), respectively, to the states $1s$ for $Z = 5$, $1s$ for $Z = 2$, $2p$, $1s$, and $3p$ (the last three for $Z = 3$).

Δ_{1s} for the ground state in the case $Z = 5$ (which explains the global shift of the spectrum to lower energies), a feature which is typical for *low* frequencies [19].

Finally, we remark that the scaling properties can also be used to predict the change of ionization mechanism (for a fixed xuv pulse of high peak intensity), from multiphoton ionization for low Z to tunnel ionization for high values of Z. Taking as example $Z = 9$, the scaled frequency corresponding to $\omega = 3.42$ a.u. is $\tilde{\omega} \approx 0.04$ a.u., a value belonging to the infrared range of frequencies. At this frequency, the onset of nonperturbative effects in the case of the hydrogen atom is expected to appear above $\tilde{I} \approx 10^{13}$ W/cm^2. However, the xuv intensity corresponding to $\tilde{I}$ is $I \approx 5.3 \times 10^{18}$ W/cm^2, a value much larger than the highest intensities for this range of frequencies, available at the present time. In the light of these considerations it is also possible to make an extrapolation to the photoionization of atoms with more than one electron in the presence of xuv pulses. For higher charge states some features encountered in the case of ionization by optical or infrared laser pulses may manifest also for xuv pulses, whenever the energy of an xuv photon is much lower than the ionization potential of these ions. As in the case of hydrogenlike atoms, the manifestation of these features may imply intensities higher than I_0. For experiments made at such intensities it is expected that the mechanisms of "atomic antenna" [20], or electron rescattering [21] will play a much more important role than in the case of experiments presented in [10,11].

V. CONCLUSIONS

We have introduced the integral representation Eq. (2) of the wave function at large distances, valid for the stage postinteraction between a one-electron atom and a short laser pulse, which contains the whole information we need to describe the photoionization process. This representation is used to give a derivation of formula (12) for the fully differential photoelectron distribution. The expression (12)

leads to a method to extract the photoelectron distributions from the time dependence of the wave function in the asymptotic region, the wave function being calculated by the numerical integration of the Schrödinger equation, on a space-time grid in our case. Our method avoids completely the calculation of the continuum incoming states. We consider the method attractive by its simplicity; it may be used efficiently together with a good propagation scheme of the wave function. The proposed procedure can be taken as a viable alternative if the incoming energy eigenfunctions are not known or too difficult to compute.

With our method, described in Sec. III, we have presented results for the photoionization of hydrogenlike atoms from the ground and several excited states, induced by the interaction with xuv laser pulses with a central wavelength of 13.3 nm, several intensities around the value I_0, and a few values of the atomic number, covering cases which, to our knowledge, are not present in the literature. These results demonstrate that for intensities of the order I_0 (or lower) the excess photon ionization is negligible in comparison with the ionization by the absorption of the minimum number of photons, a conclusion which is expected to be valid also for the photoionization of complex atomic targets. The results obtained for several values of the atomic number, consolidated by independent Floquet calculations, support the idea that the ionization of complex atoms by xuv pulses may have features (like the shift of the spectra to lower energies) which characterize the same phenomenon in the case of optical or infrared laser pulses.

ACKNOWLEDGMENTS

The author warmly thanks Viorica Florescu and Mădălina Boca for useful discussions and pertinent comments. This work was supported by the National Authority for Scientific Research, Project No. CEEX D11-39/2006, and by Consiliul National al Cercetarii Stiintifice din Invatamantul Superior-Unitatea Executiva pentru Finantarea Invatamantului Superior si a Cercetarii Stiintifice Universitare , Project No. PNII–IDEI 1909/2008.

[1] We give here only few examples: D. Bauer and P. Mulser, Phys. Rev. A **59**, 569 (1999); J. S. Parker, L. R. Moore, D. Dundas, and K. T. Taylor, J. Phys. B **33**, L691 (2000); S. Chelkowski, A. D. Bandrauk, and A. Apolonski, Phys. Rev. A **70**, 013815 (2004); C. Ruiz, L. Plaja, L. Roso, and A. Becker, Phys. Rev. Lett. **96**, 053001 (2006); T. Birkeland, M. Førre, J. P. Hansen, and S. Selstø, J. Phys. B: At. Mol. Opt. Phys. **37**, 4205 (2004).

[2] K. J. Schafer and K. C. Kulander, Phys. Rev. A **42**, 5794 (1990); H. G. Muller, *ibid.* **60**, 1341 (1999).

[3] L. B. Madsen, L. A. A. Nikolopoulos, T. K. Kjeldsen, and J. Fernández, Phys. Rev. A **76**, 063407 (2007).

[4] For relevant discussions regarding the final continuum state of systems undergoing ionization see the references: G. Breit and H. A. Bethe, Phys. Rev. **93**, 888 (1954); S. Altshuler, Nuovo Cimento **3**, 246 (1956); A. F. Starace, in *Handbuch der Physik*, Vol. 31: Corpuscles and Radiation in Matter I, edited by W. Mehlhorn (Springer, Berlin, 1982), Sec. 4; R. Szmytkowski and M. Gruchowski, J. Quant. Spectrosc. Radiat. Transfer **94**, 127 (2005).

[5] C. Pan, A. F. Starace, and C. H. Greene, Phys. Rev. A **53**, 840 (1996); P. Lambropoulos and L. A. A. Nikolopoulos, New J. Phys. **10**, 025012 (2008).

[6] L. A. A. Nikolopoulos, T. K. Kjeldsen, and L. B. Madsen, Phys. Rev. A **75**, 063426 (2007).

[7] J. Sjakste, A. G. Borisov, J. P. Gauyacq, and A. K. Kazansky, J. Phys. B: At. Mol. Opt. Phys. **37**, 1593 (2004).

[8] B. Feuerstein and U. Thumm, J. Phys. B: At. Mol. Opt. Phys. **36**, 707 (2003).

[9] A. Palacios, C. W. McCurdy, and T. N. Rescigno, Phys. Rev. A **76**, 043420 (2007).

[10] A. A. Sorokin, S. V. Bobashev, T. Feigl, K. Tiedtke, H. Wabnitz, and M. Richter, Phys. Rev. Lett. **99**, 213002 (2007).

[11] M. Richter, M. Y. Amusia, S. V. Bobashev, T. Feigl, P. N. Juranić, M. Martins, A. A. Sorokin, and K. Tiedtke, Phys. Rev. Lett. **102**, 163002 (2009).

[12] M. G. Makris, P. Lambropoulos, and A. Mihelic, Phys. Rev. Lett. **102**, 033002 (2009).

[13] The two angular integrals are equal; one can justify their equality applying the unitarity condition of the scattering. See, for example, L. Landau and E. Lifchitz, *Mécanique Quantique, Théorie non Relativiste* (Éditions Mir, Moscow, 1980), Sec. 125.

[14] B. H. Bransden and C. J. Joachain, *Introduction to Quantum Mechanics* (Longman Scientific & Technical, Essex, 1989).

[15] X. Chen, A. Sanpera, and K. Burnett, Phys. Rev. A **51**, 4824 (1995); L. Dimou and H.-J. Kull, *ibid.* **61**, 043404 (2000); see also Ref. [5].

[16] We reproduced (graphical level precision) in particular the energy spectra from (i) Fig. 5 of [6]; (ii) Fig. 1(a) (the TDSE curve) of G. Duchateau, C. Illescas, B. Pons, E. Cormier, and R. Gayet, J. Phys. B **33**, L571 (2000), and (iii) Fig. 1 of S. Dionissopoulou, T. Mercouris, A. Lyras, and C. A. Nicolaides, Phys. Rev. A **55**, 4397 (1997).

[17] L.-Y. Peng and A. F. Starace, Phys. Rev. A **76**, 043401 (2007).

[18] R. M. Potvliege, Comput. Phys. Commun. **114**, 42 (1998).

[19] R. Shakeshaft, R. M. Potvliege, M. Dörr, and W. E. Cooke, Phys. Rev. A **42**, 1656 (1990).

[20] M. Y. Kuchiev, JETP Lett. **45**, 404 (1987).

[21] P. B. Corkum, Phys. Rev. Lett. **71**, 1994 (1993).